The DOI for this manuscript is doi: 10.1175/JCLI-D-13-00017.1



Ji, X., J. Neelin, S. Lee, and C. Mechoso, 2013: Interhemispheric teleconnections from tropical heat sources in intermediate and simple models. J. Climate. doi:10.1175/JCLI-D-13-00017.1, in press.

# Interhemispheric teleconnections from tropical heat sources in intermediate and simple models

X. Ji[1], J. D. Neelin[1], S.-K. Lee[2] and C. R. Mechoso[1]

[1]*Department of Atmospheric and Oceanic Sciences, University of California, Los Angeles, California, USA*

[2]*Cooperative Institute for Marine and Atmospheric Studies, University of Miami, and NOAA/Atlantic Oceanographic and Meteorological Laboratory, Miami, Florida*



*Corresponding author address*: J. David Neelin, Department of Atmospheric and Oceanic Sciences, 7127 Math Science Building, UCLA, 405 Hilgard Avenue, Los Angeles, California, 90095-1565, USA.
*E-mail*: neelin@atmos.ucla.edu

# Abstract

The mechanisms that control the interhemispheric teleconnections from tropical heat sources are investigated using an intermediate complexity model (a Quasi-Equilibrium Tropical Circulation Model, QTCM) and a simple linear two-level model with dry dynamics. Illustrating the interhemispheric teleconnection process with an Atlantic Warm Pool principal case, the heat source directly excites a baroclinic response that spreads across the equator. Three processes involving baroclinic-barotropic interactions—shear advection, surface drag, and vertical advection—then force a cross-equatorial barotropic Rossby wave response. An analysis of these processes in QTCM simulations indicates that: (1) shear advection has a pattern that roughly coincides with the baroclinic signal in the tropics and subtropics; (2) surface drag has large amplitude and spatial extent, and can be very effective in forcing barotropic motions around the globe; (3) vertical advection has a significant contribution locally and remotely where large vertical motions and vertical shear occur. The simple model is modified to perform experiments in which each of these three mechanisms may be included or omitted. By adding surface drag and vertical advection, and comparing each to shear advection, the effects of the three mechanisms on the generation and propagation of the barotropic Rossby waves are shown to be qualitatively similar to the results in QTCM. It is also found that the moist processes included in the QTCM can feed back on the teleconnection process and alter the teleconnection pattern by enlarging the prescribed tropical heating in both intensity and geographical extent, and by inducing remote precipitation anomalies by interaction with the basic state.

# 1. Introduction

Tropical heat sources can remotely influence ocean basins and continents through atmospheric teleconnections (e.g., Horel and Wallace 1981; Ropelewski and Halpert 1987; Wallace et al. 1998; Trenberth et al. 1998). In addition to many teleconnection studies in general circulation models (GCMs; e.g., Lau 1985; Mechoso et al. 1987; Kumar and Hoerling 1998; Barnston et al. 1999; Goddard and Graham 1999; Latif et al. 1999; Saravanan and Chang 2000), much has been learned from simpler models. In the tropics, heating anomalies directly force a baroclinic signal that tends to remain trapped in latitude. Thus, highly damped shallow water models (Matsuno 1966; Webster 1972; Gill 1980), which assume a vertical structure of a single deep baroclinic mode, can give a plausible first approximation to the low-level wind field in the vicinity of heating anomalies. In mid-and high-latitudes, teleconnections tend to be dominated by an equivalent barotropic signal for two reasons. Firstly, barotropic stationary or low-frequency Rossby waves in westerly flow tend to be less equatorially trapped than their baroclinic counterparts (Salby and Garcia 1987). Secondly, vertical propagation tends to reduce the contribution of baroclinic modes in the mid-latitude troposphere, leaving the signal far from the source dominated by an equivalent barotropic mode (Held et al. 1985). Thus barotropic models have been widely used to study the teleconnection response at midlatitudes (e.g., Hoskins and Karoly 1981; Simmons 1982; Simmons et al. 1983; Held and Kang 1987). However, since the heating does not directly force a barotropic response, barotropic models used to study teleconnections must prescribe a vorticity source or "Rossby wave source" (Sardeshmukh and Hoskins 1988), which can be based, for instance, on baroclinic divergence at upper levels or on baroclinic transient motions diagnosed from a GCM simulation (Held and Kang 1987). This diagnosed Rossby wave source is one convenient approach that permits the barotropic processes to be examined while deferring investigation of the complex baroclinic to barotropic pathway in the tropics-to-midlatitudes teleconnection process. However, many of the terms that are specified as a fixed source in this approach are dynamical quantities whose scales, spatial form etc. depend on the interaction of the baroclinic mode with the basic state in ways that can be interesting to elucidate. Multi-level linear, steady-state wave models with both baroclinic and barotropic components comprise part of a model hierarchy (Hoskins and Karoly 1981; Ting and Held 1990; DeWeaver and Nigam 2004) that can capture at least some aspects of the tropical-baroclinic to midlatitude-barotropic transition. Interactions with baroclinic transient eddies (Held et al. 1989; Hoerling and Ting 1994) can also alter the teleconnection pattern in a manner that is not easily captured by stationary wave models.

The energy exchange between equatorially trapped baroclinic modes and equivalent barotropic modes with a significant projection on midlatitudes needs, therefore, to be addressed in a more sophisticated way. Instead of prescribing a Rossby wave source based on upper level divergent flow in the one level barotropic vorticity equation (e.g., Sardeshmukh and Hoskins 1988, Held and Kang 1987), a series of studies have been examining this problem from the point of view of baroclinic-barotropic interaction terms and studying the effect of each mechanism at work in the baroclinic to barotropic transition. Majda and Biello (2003) develop a set of simplified asymptotic equations describing the nonlinear interaction of near-resonant long-wavelength barotropic wave trains and equatorial baroclinic wave trains in the presence of sheared zonal mean winds, and emphasize the central role of baroclinic mean shear for sufficiently rapid nonlinear exchange of energy between the tropics and midlatitudes. Biello and Majda (2004b) further examine this resonant nonlinear interaction in the presence of vertically and meridionally sheared zonal mean winds, i.e., including both meridionally symmetric and antisymmetric (about the equator) vertical mean shear, and find that the effect of moderate antisymmetric winds is to shift the barotropic waves meridionally. Biello and Majda (2004a) incorporate the dissipative mechanisms arising from radiative cooling and atmospheric boundary layer drag, to explain how this mechanism creates barotropic/baroclinic spin up/spin down in the teleconnection process. Their results indicate that although the dissipation slightly weakens the tropics to midlatitude connection, strong localized wave packets are nonetheless able to exchange energy between barotropic and baroclinic waves on intraseasonal timescales in the presence of baroclinic mean shear. Wang et al. (2010) examine how, in the presence of background vertical shear, the transition from equatorial baroclinic mode to equivalent barotropic mode at midlatitudes establishes the interhemispheric influence of the Atlantic Warm Pool (AWP) in the northern hemisphere on the south eastern Pacific.

In this work, we aim at directly diagnosing and assessing the relative importance of the interaction terms between the baroclinic and barotropic modes that appear as source terms in the barotropic equation. These interaction terms are similar to a Rossby-wave source approach in that these terms appear as a vorticity source in the barotropic equation, but the "source" can be quantitatively and conceptually quite different than approaches based on upper level divergent flow in a single-level vorticity equation. For instance, if there is no vertical shear and no damping on the baroclinic mode associated with surface stress, then upper level divergence in the baroclinic mode does not produce any linear forcing of the barotropic mode. At the same time, by explicitly modeling the gravest baroclinic mode, the teleconnection pathway can be followed as the two modes interact, for instance with the baroclinic mode producing a teleconnection across the equator, and then interactions yielding a barotropic mode that can propagate to higher latitudes in the opposite hemisphere. Building on previous work with idealized asymptotic equations, here we use realistic background states and more detailed physics including moist processes to analyze teleconnections arising from tropical heat sources.

We use two numerical models with different complexity, in both of which the baroclinic-barotropic interactions are explicitly formulated. The more complex one is a Quasi-Equilibrium Tropical Circulation Model (QTCM) (Neelin and Zeng 2000), in which part of the quasi-equilibrium convective closure is used to carry forward analytically the model solution for the baroclinic vertical structure in the convective regions. The full primitive equations are then projected on the resulting baroclinic plus barotropic basis functions for vertical structure. This intermediate complexity model retains some of the simplicity of the analytical solutions, while keeping full nonlinearity from the primitive equations, and a consistent representation of moist processes including a deep convective parameterization. The consistent vertical mode decomposition yields three mechanisms (Neelin and Zeng 2000) for excitation terms in the barotropic equations due to baroclinic terms: interactions of vertical shear in horizontal advection terms, vertical advection of vertically sheared motions, and interactions via surface stress in the boundary layer. The QTCM thus allows for quantifying the effect of each of those mechanisms, and to assess the role of feedbacks associated with moist processes. The simpler model we use is based on that of Lee et al. 2009), which is a two-level steady-state wave model linearized about background flows. In preparation for the present study, the Lee et al. (2009) version was extended to include the three mechanisms for excitation of barotropic modes present in the QTCM. The simple model permits experiments in which mechanisms may be included or omitted. Therefore, an assessment of individual impacts is obtained by retaining the forcing terms one at a time in the barotropic equation, and inspecting the differences in the teleconnection patterns obtained with each mechanism. Our primary focus is on the heat source region above the Atlantic Warm Pool (AWP) because previous studies have shown that it has significant interhemispheric influences (e.g., Wang et al. 2010).

The remainder of the text is organized as follows. Section 2 gives a brief introduction of the two models as well as the modifications made for the study. Section 3 presents the QTCM experiments, examines each of the three forcing terms of barotropic Rossby waves, and explores the effect of moist feedback in the teleconnection process. Section 4 presents the simple model experiments, narrowing down on the role of each forcing term. Section 5 consists of a summary and discussion.

# 2. Models and Methodology

*a. QTCM*

The QTCM belongs in a class of tropical atmospheric model of intermediate complexity that occupies a niche between GCMs and simple models. In the QTCM, the derivation from the primitive equations is done systematically and the constraints placed on the baroclinic flow by the GCM convective parameterizations with quasi-equilibrium (QE) thermodynamic closures are exploited. Part of the QE convective closure can be used to carry forward analytically the model solution for the vertical structure in convective regions. Using the vertical structures based on these analytical solutions as the leading basis functions in a Galerkin projection of the primitive equations, self-consistent nonlinear terms can be retained in advection, moist convection, and vertical momentum transfer terms, among others. A more detailed model description can be found in Neelin and Zeng (2000). The model performance has been analyzed in Zeng et al. (2000) for climatology, and in Lin et al. (2000) and Lin and Neelin (2000, 2002) for intraseasonal variability. Moist teleconnection mechanisms within the tropics have been examined using this model in Su and Neelin (2002) and Neelin and Su (2005).

The present study uses the QTCM1 version 2.3 which retains a single basis function for the vertical structure of temperature. This is the simplest configuration, but with considerable success in capturing tropical phenomena, since the temperature structure matches the consequences of a quasi-equilibrium convective scheme, and the baroclinic velocity basis function is analytically compatible. This provides an appealing system for baroclinic-barotropic decomposition. One might anticipate that an additional degree of freedom in the boundary layer might alter some surface drag effects quantitatively. The numerical implementation of the QTCM1 here covers the domain from 78.75°S to 78.75°N and over all longitudes, with a horizontal resolution of 3.75° latitude and 5.625° longitude.

A brief review of the equation for the barotropic wind component in the QTCM is presented below to aid the analysis of the barotropic teleconnection process in the following sections. A summary of the QTCM1 equations are given for reference in Appendix. Using $V_0$ and $V_1$ as the basis functions for velocity, the projected barotropic vorticity equation in Neelin and Zeng (2000) is:

$$\partial_t \zeta_0 + curl_z(\mathcal{D}_{V0}(\mathbf{v_0}, \mathbf{v_1})) + \beta v_0 = -curl_z(\varepsilon_0 \mathbf{v_0}) - curl_z(\varepsilon_{10} \mathbf{v_1}) \qquad (1)$$

where subscripts 0 and 1 denote barotropic and baroclinic component, respectively, and $\mathcal{D}_{V0}(\mathbf{v_0}, \mathbf{v_1})$, the operator containing nonlinear advection terms and horizontal diffusion is given by:

$$\mathcal{D}_{V0}(\mathbf{v_0}, \mathbf{v_1}) = \mathbf{v_0} \cdot \nabla \mathbf{v_0} + \left\langle V_1^2 \right\rangle \mathbf{v_1} \cdot \nabla \mathbf{v_1} + \left\langle V_1^2 \right\rangle (\nabla \cdot \mathbf{v_1}) \mathbf{v_1} - K_H \nabla^2 \mathbf{v_0} \qquad (2)$$

where the term in brackets denote vertical averages over the troposphere $\langle X \rangle = p_T^{-1} \int_{p_{rt}}^{p_{rs}} X dp$ . For the analysis of Rossby wave sources in the QTCM, we rearrange (1) to obtain:

$$
\begin{aligned}
&\partial_t \nabla^2 \psi_0{}' + curl_z(\mathbf{v}_0 \cdot \nabla \mathbf{v}_0)' - K_H \nabla^4 \psi_0{}' + \beta v_0{}' \\
&= -curl_z(\langle V_1^2 \rangle \mathbf{v_1} \cdot \nabla \mathbf{v_1})' - curl_z(\langle V_1^2 \rangle (\nabla \cdot \mathbf{v_1}) \mathbf{v_1})' - curl_z(\varepsilon_0 \mathbf{v_0} + \varepsilon_{10} \mathbf{v_1})'
\end{aligned}
\tag{3}
$$

where $\psi_0$ is the barotropic stream function, and $()'$ denotes anomalies defined as the difference between a climatological run and a run with an imposed heating anomaly. The stationary barotropic Rossby wave response (i.e. of the l.h.s. of (3)) to a localized source is well known (e.g., Hoskins and Karoly 1981, Simmons et al. 1983; Held and Kang 1987) so we focus on the comparison of the forcing terms on the r.h.s. of (3). The three forcing sources of the barotropic motion that involve the interactions with baroclinic motion are defined as follows: 1) the shear advection term $-curl_z(\langle V_1^2 \rangle \mathbf{v_1} \cdot \nabla \mathbf{v_1})'$, which represents advective interactions of the baroclinic wind component (with vertical shear); 2) the vertical advection term $-curl_z(\langle V_1^2 \rangle (\nabla \cdot \mathbf{v_1}) \mathbf{v_1})'$, which represents the effect of vertical motion advecting the baroclinic wind component; 3) the surface drag term $-curl_z(\varepsilon_0 \mathbf{v}_0 + \varepsilon_{10} \mathbf{v}_1)'$, which derives from surface stress $-(g / p_T)\tau_s$ (with zero stress at model top) and a bulk formula parameterization $\tau_s = \tau|_{p_s} = \rho_a C_D V_s \mathbf{v_s}$. These three forcing mechanisms of the barotropic motion involved in the baroclinic-barotropic interactions are further discussed in section 3b in the teleconnection experiments. We further note that linearizing the interaction terms in (3) yields:

$$-curl_z(\langle V_1^2 \rangle \bar{\mathbf{v}}_\mathbf{1} \cdot \nabla \mathbf{v}_\mathbf{1}' + \langle V_1^2 \rangle \mathbf{v}_\mathbf{1}' \cdot \nabla \bar{\mathbf{v}}_\mathbf{1}) - curl_z(\langle V_1^2 \rangle (\nabla \cdot \mathbf{v}_\mathbf{1}') \bar{\mathbf{v}}_\mathbf{1} + \langle V_1^2 \rangle (\nabla \cdot \bar{\mathbf{v}}_\mathbf{1}) \mathbf{v}_\mathbf{1}') - curl_z(\varepsilon_0 \mathbf{v}_\mathbf{0}' + \varepsilon_{10} \mathbf{v}_\mathbf{1}') .$$

The linearized interaction terms make it clear that if there is no vertical shear or vertical velocity in the mean state ($\bar{\mathbf{v}}_1 = 0$) and no drag on the baroclinic mode ($\varepsilon_{10} = 0$), then the baroclinic mode can have any vertical velocity ($\nabla \cdot \mathbf{v}_1'$), but there will be no forcing of the barotropic mode. This appears quite different from the assumptions used in traditional Rossby wave source approaches based on a vorticity equation at upper levels, but is similar in the sense that it diagnoses a vorticity source that drives the barotropic equation, in this case the equation for the full barotropic mode. We will refer to this as a "barotropic Rossby wave source" for clarity since it is the vorticity source term as it occurs projected on the full barotropic mode We also note that while we have retained the whole surface stress term on the right-hand side above, arguably it is more consistent to move the barotropic component of this, i.e., $-curl_z(\varepsilon_0 \mathbf{v}_0')$, to the l.h.s. in (3) since it acts as a drag on the barotropic mode. In that case the surface drag contribution to the barotropic Rossby wave source due to the baroclinic mode is simply $-curl_z(\varepsilon_{10} \mathbf{v}_1')$. We will show examples of both in diagnostics.

### *b. Simple model*

The simple model we use in this study is based on that developed by Lee et al. (2009). This is a two-level model, in which equations are recast as baroclinic and barotropic components, and are linearized about prescribed background wind fields. The model is designed to simulate both the local and remote stationary response of the atmosphere when forced with a localized heating. In this model, the baroclinic response to tropical heating anomalies is essentially the same as described by the Matsuno-Gill model (Matsuno 1966; Gill 1980) with damping used in Lee et al (2009). This baroclinic response then excites a barotropic response by advective interactions with vertical background wind shear (i.e., through the shear advection mechanism), and the barotropic signals are in turn transmitted to high latitudes.

Our modification of the Lee et al. (2009) model allows for consideration of surface drag as another mechanism of baroclinic-barotropic interactions. This was done by eliminating, from the relative vorticity equations, the linear momentum damping $-r\nabla^2\psi$ both in the upper (250mb) and lower (750mb) levels, and adding in the lower level a term $-r_s\nabla^2\psi$, where the surface drag coefficient is $r_s=(g/p_T)\rho_a C_D V_s$. Thus, in the barotropic and baroclinic vorticity equations, the linear damping coefficients $r_0$ and $r_1$ become $r_0=r_1=r_s/2$. We set $r_s=(3.5\text{day})^{-1}$ for $p_T=500\text{mb}, C_D=10^{-3}, V_s=10\text{m s}^{-1}$. The simple model (as modified relative to Lee et al 2009) is thus given by the following barotropic and baroclinic vorticity equations:

$$\frac{1}{a\cos\theta}\left[\frac{\partial}{\partial\lambda}(\bar{u}_0\nabla^2\psi_0'+u_0'\nabla^2\bar{\psi}_0)+\frac{\partial}{\partial\theta}(\cos\theta\bar{v}_0\nabla^2\psi_0'+\cos\theta v_0'\nabla^2\bar{\psi}_0)\right]+2\Omega\frac{v_0'}{a} = -r_0\nabla^2\psi_0'+r_0\nabla^2\psi_1'+A_0\nabla^4\psi_0'+F_{\psi_0} \tag{4}$$

$$\frac{1}{a\cos\theta}\left[\frac{\partial}{\partial\lambda}(\bar{u}_1\nabla^2\psi_1'+u_1'\nabla^2\bar{\psi}_1)+\frac{\partial}{\partial\theta}(\cos\theta\bar{v}_1\nabla^2\psi_1'+\cos\theta v_1'\nabla^2\bar{\psi}_1)\right]+2\Omega\frac{v_1'}{a} = -r_1\nabla^2\psi_1'+r_1\nabla^2\psi_0'+A_1\nabla^4\psi_1'+F_{\psi_1} \tag{5}$$

where subscripts 0 and 1 denote barotropic and baroclinic mode respectively, variables are separated into the basic state and anomaly components denoted by bar and prime terms, $A_0$ and $A_1$ are the momentum diffusion coefficient for barotropic and baroclinic motion respectively. The differences from the model in Lee et al. (2009) are the two terms $r_0\nabla^2\psi_1'$ and $r_1\nabla^2\psi_0'$ that derive from the surface drag mechanism. The $F_\psi$ terms represent the vorticity tendency terms due to the shear advection and vertical advection mechanisms of baroclinic-barotropic interactions. The complete form of $F_{\psi_0}$ is:

$$F_{\psi_0} = \frac{1}{a\cos\theta}\left[\frac{\partial}{\partial\lambda}(\overline{u}_1\nabla^2\psi_1' + u_1'\nabla^2\overline{\psi}_1) + \frac{\partial}{\partial\theta}(\cos\theta\overline{v}_1\nabla^2\psi_1' + \cos\theta v_1'\nabla^2\overline{\psi}_1)\right]$$
$$= \frac{1}{a\cos\theta}\left\{\begin{array}{l}\nabla^2\psi_1'\left[\frac{\partial\overline{u}_1}{\partial\lambda} + \frac{\partial}{\partial\theta}(\cos\theta\overline{v}_1)\right] + \nabla^2\overline{\psi}_1\left[\frac{\partial u_1'}{\partial\lambda} + \frac{\partial}{\partial\theta}(\cos\theta v_1')\right] \\ + \left[\overline{u}_1\frac{\partial\nabla^2\psi_1'}{\partial\lambda} + \overline{v}_1\frac{\partial}{\partial\theta}(\cos\theta\nabla^2\psi_1')\right] + \left[u_1'\frac{\partial\nabla^2\overline{\psi}_1}{\partial\lambda} + v_1'\frac{\partial}{\partial\theta}(\cos\theta\nabla^2\overline{\psi}_1)\right]\end{array}\right\} \quad (6)$$

The first term in the r.h.s. of (6) represents the vertical advection of anomalous baroclinic vorticity via background vertical wind. The second term represents the vertical advection of background baroclinic vorticity via anomalous vertical wind. The third term represents the zonal and meridional advection of anomalous baroclinic vorticity via background zonal and meridional shear. The fourth term represents the zonal and meridional advection of background baroclinic vorticity via anomalous zonal and meridional shear.

The thermodynamic equation is given by:

$$\gamma\phi_1 + c_g^2\nabla^2\chi_1 = -Q \quad (7)$$

where $\gamma$ is the thermal damping coefficient, $\phi_1$ is the baroclinic geopotential, $c_g$ is the internal gravity wave speed, $\chi_1$ is the baroclinic divergence and $Q$ is the diabatic heating rate. Note that the simple model is explicitly steady state and linear and omits all moisture effects. The equations (4)-(7) together with a baroclinic divergence equation (not shown here) are in a closed form and are the governing equations solved in the simple model.

In our simple model experiments, we are able to activate and deactivate each forcing mechanism—the surface drag, the vertical advection and the shear advection, and compare the effects of each forcing with those in the QTCM results.

The numerical implementation of the three versions of the simple model covers the domain from 90°S to 90°N over all longitudes, with a horizontal resolution of 4.5° latitude and 4.5° longitude.

### *c. Methodology*

We concentrate on the period of June-August (JJA), during which the tropical heating and precipitation anomalies develop to their maximum strength in the northern hemisphere summer, including in the AWP region of interest here. In JJA, the subtropical jets are strong in the southern (winter) hemisphere, which can favor the shear advection mechanism for interhemispheric teleconnections (Wang et al. 2010). Accordingly, in both the QTCM and simple model, the zonal mean of the barotropic and baroclinic wind fields are prescribed as the JJA zonal means. The time advance of the zonal mean fields in the QTCM is, therefore, bypassed. The prescribed velocities correspond to the streamfunction at the 250 and 750mb levels from the monthly NCEP-NCAR reanalysis (Kalnay et al. 1996):

$$\bar{u}_0 = -\frac{\partial}{\partial y}\bar{\psi}_0^{ncep} = -\frac{\partial}{\partial y}[(\bar{\psi}_{250}^{ncep} + \bar{\psi}_{750}^{ncep})/2] \tag{8}$$

$$\bar{u}_1 = -\frac{\partial}{\partial y}\bar{\psi}_1^{ncep} = -\frac{\partial}{\partial y}[(\bar{\psi}_{250}^{ncep} - \bar{\psi}_{750}^{ncep})/2] \tag{9}$$

Further, in the QTCM we replace the zonal velocity that advects the temperature gradient by that corresponding to the zonal mean basic state velocity as in equations (8) and (9). This procedure removes the main source term for baroclinic instability, thus reducing weather variability. There are some trade-offs here. On the one hand, due to reduction in poleward fluxes, more moisture is available for precipitation in the subtropics, and interactions of the teleconnections with storm tracks are suppressed. On the other hand, the procedure has several advantages in view of our goals. These include (i) statistically significant signals are easy to detect in decadal runs, (ii) comparison to the simple model is facilitated, (iii) the basic state on which wave propagation occurs is strongly constrained towards observations, and (iv) interpretation in terms of stationary wave propagation is more straightforward. This should thus be viewed as an intermediate step between simple models and GCMS that would potentially include more complex effects such as interaction with baroclinic transients.

# 3. QTCM Experiments and Results

*a. Atlantic Warm Pool (AWP) teleconnection experiments set up*

In this experiment, we prescribe a Gaussian-shaped baroclinic heating anomaly as in Lee et al. (2009). The anomaly amplitude is $169.2 W/m^2$ (which is equivalent to 6mm/day of precipitation) at the center at (20°N, 70°W), and the zonal and meridional length scales are 5° latitude and 15° longitude (see Fig. 1a). The model is then run for ten years using monthly climatological SSTs (Reynolds and Smith 1994).

Figure 1b shows the precipitation response averaged over the June-August for ten years in response to the prescribed heating anomalies in this experiment. It can be seen that the latent heat associated with the precipitation anomalies enhance the local prescribed heating anomalies to a significant extent, and thus will enhance the teleconnection response in comparison to a model with dry dynamics. The shape of the heating is also slightly modified from the prescribed. We return to this moist feedback effect in section 3c.

*b. AWP teleconnections analysis*

The JJA mean baroclinic and barotropic streamfunctions anomalies are shown in Figs. 2a and 2b. The baroclinic mode resembles the Gill–Matsuno-type response (Matsuno 1966; Gill 1980) and is equatorially trapped with most of the signal within equatorial deformation radius. An important aspect is that the off-equatorial heating projects sufficiently on the Kelvin mode (to the east of the heating) and the symmetric Rossby modes (to the west) that a substantial baroclinic signal crosses the equator. The barotropic mode shows an interesting pattern. Typically, a pure barotropic stationary Rossby wave propagating in a westerly region of the mid-latitudes in an approximately barotropic basic state will approach a critical latitude where $\bar{u} = 0$ and thus will not propagate directly across the region of easterlies near equator. In our experiments, however, the barotropic signal has a significant component in the southern hemisphere. This is because the QTCM includes a full set of forcing sources of the barotropic motions through baroclinic-barotropic interactions. As mentioned in section 2a, in the model's barotropic component equation in QTCM, the three baroclinic forcing mechanisms—the shear advection, surface drag, and vertical advection— actively generate barotropic wave trains in the equatorial regions and within the southern hemisphere westerlies.

To explore the relative importance of the three mechanisms of interest in the QTCM AWP experiment, we plot in Figs. 3a, 3b, 3c the amplitudes of the three terms in the r.h.s. of (3), and in Figs. 4a, 4b, 4c their inverse Laplacians, i.e., the equivalent barotropic streamfunction tendency terms. Shaded areas in Figs 3 and 4 represent values that are statistically significant with a confidence level of 99% from a student's t-test. The shear advection term $-curl_z(\langle V_1^2 \rangle \mathbf{v_1} \cdot \nabla \mathbf{v_1})'$ shows a large dipole in the tropics (Fig. 3a and 4a), roughly coincident with where the baroclinic signal is strong. The southwest to northeast angle reflects the corresponding tilt seen in Fig. 2 close to the zero contour of $\psi_1$ where the strong gradient in $\psi_1$ indicates strong baroclinic wind anomalies. Thus the region of strong shear forcing reflects the heating-forced baroclinic anomalies which, while equatorially trapped, are able to propagate into the southern hemisphere where they can excite barotropic waves.

The magnitude of the surface drag term $-curl_z(\varepsilon_0 \mathbf{v}_0 + \varepsilon_{10} \mathbf{v}_1)'$ in Fig. 3b is not locally as large as that of the shear advection term (Fig. 3a) and vertical advection term (Fig. 3c), but its inverse Laplacian (Fig. 4b) shows large values around the heat source with amplitudes comparable with the vertical advection term. The geographical spread of the surface drag forcing is broader in both hemispheres than the two other mechanisms. Note that Figs. 3b and 4b show the net effect of surface drag mechanism, i.e., the amplitude of the baroclinic forcing $-curl_z(\varepsilon_{10} \mathbf{v}_1')$ after compensation by linear damping $-curl_z(\varepsilon_0 \mathbf{v}_0')$. Also note that the sign of the coefficient of transfer by surface stress between baroclinic and barotropic wind components $\varepsilon_{10}$ is negative in order that all the turbulence terms have the same form (refer to the appendix for more detail). For a rough estimate of this compensation, comparing the amplitudes of $-\varepsilon_{10}\psi_1$ (where $\varepsilon_{10} = (-28\text{day})^{-1}$ and $\psi_1$ can be approximated from the values in Fig. 2a) and $-\varepsilon_0\psi_0$ (where $\varepsilon_0 = (5.6\text{day})^{-1}$ and $\psi_0$ can be approximated from the values in Fig. 2b), indicates that the compensation effect of the linear damping can be as large as 50% of the baroclinic forcing. This estimate is confirmed by Fig. 3d, showing only the baroclinic forcing component of the surface drag $-curl_z(\varepsilon_{10}\mathbf{v}_1')$. As expected, this component is roughly twice as large locally as the total surface drag term (Fig. 3b). We can also see that the surface drag component has a significant contribution in the southern hemisphere. Thus the baroclinic forcing from the surface drag term can potentially exert a substantial impact on the generation and propagation of barotropic Rossby waves, especially in the southern hemisphere corresponding to the $\psi_1$ response there.

Finally, the vertical advection term $-curl_z(\langle V_1^2 \rangle(\nabla \cdot \mathbf{v_1})\mathbf{v_1})'$ (Figs. 3c and 4c) shows a localized forcing around the heat source where the vertical velocity is large (also see Fig. 1b for large local precipitation anomaly there). Note that some degree of compensation can occur with the surface drag term in regions of upward vertical motion where the vertical velocity term contribution $-\langle V_1^2 \rangle(\nabla \cdot \bar{\mathbf{v}}_1) curl_z \mathbf{v}_1'$ has opposite sign but similar form to $-curl_z(\varepsilon_{10}\mathbf{v}_1')$. Far from the heat source, in certain regions of the Pacific and Indian Ocean, the vertical velocity term can still have fairly substantial contributions corresponding to the remote precipitation anomalies in those regions. The strong vertical advection forcing locally around the heat source (Fig. 3c) and the remote signals in the southern hemisphere imply that this mechanism has a substantial role in the interhemispheric teleconnections, and should not be neglected.

### *c. Moist feedback*

The precipitation response in the QTCM AWP experiments is shown in Fig. 1b. There is clear evidence that moist processes enhance the teleconnection process. First, moist feedback enhances the prescribed anomalous heat source locally by approximately 6mm/day in this experiment, which is as large as the prescribed heat source. Second, the shape of the precipitation anomaly is stretched southwestward into eastern Pacific region. A similar feature is apparent in the GCM AWP experiments in Wang et al. (2007, 2008). This precipitation anomaly is the result of the Atlantic Warm Pool-induced subtropical Rossby waves propagating westward and interacting with the Intertropical Convergence Zone (ITCZ) in the eastern Pacific. The impact of this convective heating anomaly in the eastern Pacific is further analyzed in section 3d. Third, this elongated shape, and the compensating subsidence north of the precipitation anomaly are consistent with the mechanism described in Chou and Neelin (2003) as the result of the interaction between baroclinic Rossby wave dynamics and convective heating. The subsidence may modestly impact the teleconnection patterns north of the heating anomaly by reducing the baroclinic signal extent and by contributing to vertical advection. Finally, as the flow anomalies produced by the teleconnections interact with moist processes remotely, e.g., advecting the basic state moisture gradient, they can induce remote precipitation anomalies that can contribute to the baroclinic-barotropic interaction. For instance, Fig. 1b shows precipitation anomalies in the equatorial Western Pacific and in the subtropical Southeastern Pacific. The latter corresponds to a significant contribution to the vertical advection forcing term in Figs. 3c and 4c in the southern hemisphere.

### *d. The impact of the response in the eastern Pacific ITCZ region*

As mentioned in section 3c, the moist feedback on the teleconnections leads to an elongation of the anomalous heat source in the AWP region into the eastern Pacific ITCZ region. This elongation is also seen in the AGCM experiments of Want et al. (2007, 2008). Here, we investigate quantitatively the influence of this additional heating in the ITCZ region on the AWP teleconnections into the southern hemisphere. We prescribe a similar Gaussian-shaped baroclinic heating anomaly with the same amplitude as in the one above the AWP, but with the center at

(15°N, 95°W), and scales of 3.0° latitude and 7.5° longitude. The model is then run for ten years using monthly climatological SSTs (Reynolds and Smith 1994).

Fig. 5 shows the barotropic streamfunction response to the heating prescribed in the eastern Pacific region. A comparison between this and Fig. 2b, reveals an overlap of the positive and negative phases of the response induced by the two different heating regions, and confirms that the induced eastern Pacific heating provides a positive feedback to the original AWP heating. We have also tested the result's sensitivity to the extension of the elongation, and found that the model response to a further elongation into the eastern Pacific as that in the AGCM experiments of Want et al. (2007, 2008) has an extremely similar pattern (not shown).

e. *Sensitivity of the teleconnection pattern to longitudinal location of heating anomaly*

To explore the dependence of the teleconnection response to the heating location in longitude, we perform a supplementary experiment in which the heating source is placed in the central Pacific at a location 90° in longitude west of the AWP (see Fig. 6a). The precipitation anomalies in this experiment are shown in Fig. 6b, while the baroclinic and barotropic streamfunctions response are shown in Figs. 7a and 7b, respectively. The zonally asymmetric basic state in the model can affect wave propagation, but some of the most obvious differences arise in the moist response to the source. The precipitation anomalies do not show a similar elongation as those in the AWP experiment (Fig. 1b), which leads to smaller zonal wavelengths in the baroclinic and hence in the barotropic response (Fig. 7b). Based on the WKB theory for stationary barotropic Rossby wave propagation in latitudinally varying flow, the local meridional wave number $l(y)$ is given by $l(y) = \pm(\hat{\beta}\overline{u}_m^{-1} - k^2)^{1/2}$, where $k$ is the zonal wave number, $\hat{\beta}$ and $\overline{u}_m$ are basic state vorticity and zonal mean flow variables defined in Mercator coordinates equivalent to the form on a beta-plane with spherical effects incorporated (Hoskins and Karoly 1981). The smaller zonal wavelengths (larger zonal wave number $k$ ) mean a lower turning latitude because the local meridional wave number for stationary barotropic Rossby waves goes to zero at smaller values of $\hat{\beta}\overline{u}_m^{-1}$. Thus the wave arc in the northern hemisphere is more zonal. In the southern hemisphere, the barotropic responses in both the AWP and central Pacific experiments (Figs. 2b and 7b) are qualitatively similar, but the latter one has weaker magnitudes. This is partly due to the small baroclinic response in the southern hemisphere (Fig. 7a), and to the absence of the vertical advection forcing sources in the southern Pacific (Figs. 3c and 4c).

# 4. Simple Model experiments

In the simple model, an identical Gaussian-shaped heating anomaly is prescribed in the AWP region with a diabatic heating rate of $2.5\times10^{-2}\,\mathrm{W\,kg^{-1}}$ , which is equivalent to $2.15\ \mathrm{K\ day^{-1}}$ at 500mb. For the simple vertical structure of this model (linear within each layer), this would be roughly equivalent to $127.6\ \mathrm{W\,m^{-2}}$ using 500mb layer depth. This heating anomaly is the only heat source since there is no moist feedback in the model. Recall from section 2, that the model is linearized about the basic state from JJA NCEP-NCAR reanalysis streamfunction averaged zonally around the globe. Other model parameters used in the present study are the same as those in Lee et al. (2009) with the following exceptions. The barotropic and baroclinic linear damping coefficient is set to $(3.5\mathrm{day})^{-1}$ for compatibility with the QTCM; and the barotropic horizontal mixing coefficient is set to $2.5\times10^{5}\,\mathrm{m^2s^{-1}}$ following Wang et al (2010). Altering these damping coefficients affects the rate at which the barotropic wave decays.

Figures 8a shows the barotropic streamfunctions response in the model with shear advection mechanism, and Fig. 8b shows the corresponding values with both shear advection and surface drag mechanisms included (Note that the latitude coverage is adjusted to 78.75°S to 78.75°N in order to compare with the QTCM results). Addition of the surface drag mechanism results in a strong amplification and extension of the barotropic response in the southern hemisphere. This supports the finding in the QTCM experiments that the surface drag mechanism is potentially very effective in forcing the barotropic response globally, especially in spreading the cross-equatorial barotropic signals.

Figure 8c shows the barotropic streamfunction response of the model experiment with both the shear advection and the vertical advection mechanisms. Comparing with Fig. 8a, as in the QTCM experiment, the vertical advection amplifies the barotropic response locally around the heating area, and spreads the barotropic signals into the southern hemisphere, although the impact is moderate compared to the surface drag mechanism.

# 5. Summary and discussion

We have investigated the mechanisms that control the interhemispheric teleconnections from tropical heat sources. Our approach is based on the analysis of the response to idealized distributions of tropical heating sources in experiments in QTCM and in a simple steady-state, damped, linear stationary wave model. We concentrated primarily in the Atlantic Warm Pool region to prescribe the heating because it has been identified as significant in setting up interhemispheric influence in previous studies (e.g., Wang et al. 2010). The direct baroclinic response to this tropical heating is approximately a Gill–Matsuno-type response (Matsuno 1966;

Gill 1980), which is equatorially trapped. The teleconnections to mid and high latitudes are dominated by barotropic mode. The baroclinic to barotropic pathway is complex involving the basic state shear with all its spatial dependence, as well as the basic state vertical velocity and surface drag. In absence of basic state shear and vertical velocity and of surface drag, baroclinic and barotropic components are decoupled. This makes the recent literature examining the role of these interaction terms as a driver for barotropic motions from heat forced baroclinic motions (e.g., Neelin and Zeng 2000, Majda and Biello 2003, Lee et al. 2009) appear very different from the earlier literature that assumed upper-level divergence and related terms could be viewed as a driver (e.g., Sardeshmukh and Hoskins 1988, Held and Kang 1987), often summarized as a vorticity source term (the "Rossby wave source") for a single-level barotropic equation. Here we diagnose the interaction terms as a consistent vorticity source for the barotropic mode in a primitive equation model that has an explicit vertical mode decomposition. In addition to explicit computation of the interaction terms as in earlier theoretical studies, the study retains a complex three-dimensional basic state and moist processes for a quantitative examination.

The interaction-term framework results in some very substantial differences in the way one views the teleconnections generated by anomalous heating. First, it should be noted that upper-level divergence in the baroclinic mode does not necessarily drive a response in the barotropic mode, as is commonly assumed, unless appropriate conditions such as basic state shear occur in the regions of descent. Furthermore, for interhemispheric teleconnections or tropical to mid-latitude teleconnections, the first leg of the teleconnection occurs in the baroclinic mode. Equatorially trapped baroclinic waves can be responsible for most of the propagation within regions where low-frequency barotropic modes are evanescent, including across the equator. Diagnosis of interaction terms as a forcing in the barotropic equation in the QTCM results then allows us to identify the relative importance of each mechanism in exciting the barotropic mode: the shear advection mechanism, the surface drag mechanism and the vertical advection mechanism. In these results, the Rossby wave source in the barotropic equation due to shear advection roughly coincides with the baroclinic signal in the tropics and subtropics, and thus can be effective in contributing to the southern hemisphere response to an Atlantic Warm Pool heat source. The barotropic Rossby wave source due to surface drag is more broadly spatially spread, essentially reflecting the contribution of the baroclinic mode to low-level wind, and has large enough magnitude to provide a substantial forcing mechanism for interhemispheric teleconnections. Last, the barotropic Rossby wave source due to vertical advection is significant in locations where the climatological vertical velocity and vertical shear are both large. These mechanisms were further examined by modifying the simple model to include the surface drag and vertical advection one by one, and by comparing their effects with the shear advection mechanism. The results from the simple model provide support to the interpretation of QTCM results.

The QTCM results also allowed for an assessment of effects that moist feedbacks can have in such interhemispheric teleconnections. Moist processes strengthen the initial heating locally. In the Atlantic Warm Pool experiment, the region of anomalous heating is extended westward by the induced precipitation anomalies in the Eastern Pacific ITCZ region. This amplifies the original teleconnection response, as shown if these anomalies are applied separately. Such an effect depends on the regional basic state: it does not occur for a similar initial anomaly applied in the central Pacific. Additional moist feedbacks can occur remotely. In the Atlantic warm pool experiment, induced precipitation anomalies are obtained in both the equatorial Western Pacific and the subtropical Eastern Pacific. The latter contribute to the vertical advection forcing of barotropic motions in the southern hemisphere. The total moist feedback on the teleconnection process is thus able to alter significantly the teleconnection response to tropical heating.

*Acknowledgments*

We thank Joyce Meyerson and Katrina Hales in their help and support in running the QTCM. We also thank Joyce Meyerson for her graphical work for this paper. This work was supported by National Science Foundation Grant AGS-1102838 and AGS-1041477.

# APPENDIX

## QTCM equations

QTCM is a nonlinear tropical circulation model that makes use of constraints from a particular QE convective scheme, the Betts-Miller scheme, but does not assume that convective QE has to hold. To achieve this, temperature, velocity and moisture are expanded in terms of a truncated series of basis functions in the vertical:

$$T = T_r(p) + \sum_{k=1}^{K} a_k(p) T_k(x, y, t) \tag{A1}$$

$$\mathbf{v} = \sum_{k=0}^{L} V_k(p) \mathbf{v}_k(x, y, t) \tag{A2}$$

$$q = q_r(p) + \sum_{k=1}^{K} b_k(p) q_k(x, y, t) \tag{A3}$$

The model simply takes analytical solutions that hold approximately under QE conditions and employs them as leading basis functions to represent the vertical structure of the flow.

For the standard version of QTCM1, a single deep convective mode is retained in the vertical thermodynamic structure (i.e., $T = T_r(p) + a_1(p)T_1(x,y,t)$) with two components (barotropic $V_0(p)$ and baroclinic $V_1(p)$) in the vertical structure of velocity. Discretization of the moisture equation is largely independent. The model simply chooses a truncation for the moisture equation to have a similar level of complexity as for the temperature equation.

Using $V_0$ and $V_1$ as the basis functions, the momentum equations are projected onto these (i.e., taking the inner product of the momentum equation with $V_0$ and $V_1$ respectively) to obtain the prognostic equations for barotropic wind component and baroclinic wind component:

$$\partial_t \zeta_0 + curl_z(\mathcal{D}_{V0}(\mathbf{v_0}, \mathbf{v_1})) + \beta v_0 = -curl_z(\varepsilon_0 \mathbf{v_0}) - curl_z(\varepsilon_{10} \mathbf{v_1}) \tag{A4}$$

$$\partial_t \mathbf{v}_1 + \mathcal{D}_{V1}(\mathbf{v_0}, \mathbf{v_1}) + f\mathbf{k} \times \mathbf{v}_1 = -\kappa \nabla T_1 - \varepsilon_1 \mathbf{v}_1 - \varepsilon_{01} \mathbf{v}_0 \tag{A5}$$

where the advection-diffusion operators are given by:

$$\mathcal{D}_{V0}(\mathbf{v_0}, \mathbf{v_1}) = \mathbf{v_0} \cdot \nabla \mathbf{v_0} + \langle V_1^2 \rangle \mathbf{v_1} \cdot \nabla \mathbf{v_1} + \langle V_1^2 \rangle (\nabla \cdot \mathbf{v_1}) \mathbf{v_1} - K_H \nabla^2 \mathbf{v_0} \tag{A6}$$

$$\mathcal{D}_{V1}(\mathbf{v_0}, \mathbf{v_1}) = \mathbf{v_0} \cdot \nabla \mathbf{v}_1 + \frac{\langle V_1^3 \rangle}{\langle V_1^2 \rangle} \mathbf{v_1} \cdot \nabla \mathbf{v_1} + \mathbf{v}_1 \cdot \nabla \mathbf{v}_0 - (\langle V_1 \Omega_1 \partial_p V_1 \rangle / \langle V_1^2 \rangle)(\nabla \cdot \mathbf{v_1}) \mathbf{v_1} - K_H \nabla^2 \mathbf{v}_1 \tag{A7}$$

vertical averages over the troposphere are defined as:

$$\hat{X} = \langle X \rangle = p_T^{-1} \int_{p_{rt}}^{p_{rs}} X dp \tag{A8}$$

and $\Omega_1(p)$ represents the vertical structure of vertical velocity from the baroclinic wind. Because vertical velocity is diagnostic in the primitive equations, solving the continuity equation gives:

$$\omega_1(x,y,p,t) = -\Omega_1(p)\nabla\cdot\mathbf{v}_1(x,y,t) \tag{A9}$$

$$\text{and} \quad \Omega_1(p) = -\int_p^{p_s} V_1(p)dp \tag{A10}$$

Two of the terms arising from vertical transfer of momentum to surface stress by parameterized subgrid-scale turbulence in the barotropic equation are defined as:

$$\varepsilon_0 = (g/p_T)\rho_a C_D V_s \tag{A11}$$

$$\varepsilon_{10} = (g/p_T)\rho_a C_D V_s V_{1s} \tag{A12}$$

where $V_s$ is calculated as $\sqrt{u_s^2 + v_s^2 + V_{s\min}^2}$ , and $V_{1s}$ is value of the baroclinic basis function $V_1$ at surface. The surface drag coefficient $C_D$ changes according to land surface type. The sign of $\varepsilon_0$ and $\varepsilon_{10}$ are set as opposite in the model in order that the two surface drag terms has the same form.

Vertically integrating the temperature and moisture equations from the standard nonlinear primitive equations, with vertical velocity and velocity truncated at $V_1$ yields:

$$\hat{a}_1(\partial_t + \mathcal{D}_{T1})T_1 + M_{S1}\nabla\cdot\mathbf{v}_1 = \langle Q_c\rangle + (g/p_T)\times(-R_t^{\uparrow} - R_s^{\downarrow} + R_s^{\uparrow} + S_t - S_s + H) \tag{A13}$$

$$\hat{b}_1(\partial_t + \mathcal{D}_{q1})q_1 + M_{q1}\nabla\cdot\mathbf{v}_1 = \langle Q_q\rangle + (g/p_T)E \tag{A14}$$

where the advection-diffusion operators are, respectively:

$$\mathcal{D}_{T1} = \mathbf{v}_0\cdot\nabla + \hat{a}_1^{-1}\langle a_1 V_1\rangle\mathbf{v}_1\cdot\nabla - K_H\nabla^2 \tag{A15}$$

$$\mathcal{D}_{q1} = \mathbf{v}_0\cdot\nabla + \hat{b}_1^{-1}\langle b_1 V_1\rangle\mathbf{v}_1\cdot\nabla - K_H\nabla^2 \tag{A16}$$

and the dry static stability $M_{S1}$ and the gross moisture stratification $M_{q1}$ are given by, respectively:

$$M_{S1} = p_T^{-1} \int_{p_{rt}}^{p_{rs}} \Omega_1 (-\partial_p s) dp \tag{A17}$$

$$M_{q1} = p_T^{-1} \int_{p_{rt}}^{p_{rs}} \Omega_1 (-\partial_p q) dp \tag{A18}$$

where $s = T + \phi$ is the dry static energy, with $\phi$ the geopotential. The moist convective parameterization projects the Betts – Miller scheme onto the basis functions of temperature and moisture, resulting in:

$$\langle Q_c \rangle = -\langle Q_q \rangle = \varepsilon_c^* (q_1 - T_1) \tag{A19}$$

where $\varepsilon_c^* \equiv \hat{a}_1 \hat{b}_1 (\hat{a}_1 + \hat{b}_1)^{-1} \varepsilon_c$ and $\varepsilon_c = \tau_c^{-1} \mathscr{H}(C_1)$, with $\tau_c$ the convective adjustment time, $\mathscr{H}(C_1)$ a Heaviside function that represents the dependence of convection on conditional instability in the column, and $C_1$ a measure of CAPE for this model. Detailed treatment and parameterization of other terms on the right hand side of the temperature and moisture equations can be found in Neelin and Zeng (2000).

# References

Barnston, A. G., and Coauthors, 1999: NCEP forecasts of the El Nino of 1997-98 and its US impacts. *B Am Meteorol Soc*, **80,** 1829-1852.

Biello, J. A., and A. J. Majda, 2004a: Boundary layer dissipation and the nonlinear interaction of equatorial baroclinic and barotropic Rossby waves. *Geophys Astro Fluid*, **98,** 85-127.

——, 2004b: The effect of meridional and vertical shear on the interaction of equatorial baroclinic and barotropic Rossby waves. *Stud Appl Math*, **112,** 341-390.

Chou, C., and J. D. Neelin, 2003: Mechanisms limiting the northward extent of the northern summer monsoons over North America, Asia, and Africa. *J Climate*, **16,** 406-425.

DeWeaver, E., and S. Nigam, 2004: On the Forcing of ENSO Teleconnections by Anomalous Heating and Cooling. *J Climate*, **17,** 3225-3235.

Gill, A. E., 1980: Some Simple Solutions for Heat-Induced Tropical Circulation. *Q J Roy Meteor Soc*, **106,** 447-462.

Goddard, L., and N. E. Graham, 1999: Importance of the Indian Ocean for simulating rainfall anomalies over eastern and southern Africa. *J Geophys Res-Atmos*, **104,** 19099-19116.

Held, I. M., and I. S. Kang, 1987: Barotropic Models of the Extratropical Response to El-Nino. *J Atmos Sci*, **44,** 3576-3586.

Held, I. M., R. L. Panetta, and R. T. Pierrehumbert, 1985: Stationary External Rossby Waves in Vertical Shear. *J Atmos Sci*, **42,** 865-883.

Held, I. M., S. W. Lyons, and S. Nigam, 1989: Transients and the Extratropical Response to El-Nino. *J Atmos Sci*, **46,** 163-174.

Hoerling, M. P., and M. F. Ting, 1994: Organization of Extratropical Transients during El-Nino. *J Climate*, **7,** 745-766.

Horel, J. D., and J. M. Wallace, 1981: Planetary-Scale Atmospheric Phenomena Associated with the Southern Oscillation. *Mon Weather Rev*, **109,** 813-829.

Hoskins, B. J., and D. J. Karoly, 1981: The Steady Linear Response of a Spherical Atmosphere to Thermal and Orographic Forcing. *J Atmos Sci*, **38,** 1179-1196.

Kalnay, E., and Coauthors, 1996: The NCEP/NCAR 40-year reanalysis project. *B Am Meteorol Soc*, **77,** 437-471.

Kumar, A., and M. P. Hoerling, 1998: Specification of regional sea surface temperatures in atmospheric general circulation model simulations. *J Geophys Res-Atmos*, **103,** 8901-8907.

Latif, M., D. Dommenget, M. Dima, and A. Grotzner, 1999: The role of Indian Ocean sea surface temperature in forcing east African rainfall anomalies during December-January 1997/98. *J Climate*, **12,** 3497-3504.

Lau, N. C., 1985: Modeling the Seasonal Dependence of the Atmospheric Response to Observed El-Ninos in 1962-76. *Mon Weather Rev*, **113,** 1970-1996.

Lee, S. K., C. Z. Wang, and B. E. Mapes, 2009: A Simple Atmospheric Model of the Local and Teleconnection Responses to Tropical Heating Anomalies. *J Climate*, **22,** 272-284.

Lin, J. W. B., and J. D. Neelin, 2000: Influence of a stochastic moist convective parameterization on tropical climate variability. *Geophys Res Lett*, **27,** 3691-3694.

——, 2002: Considerations for stochastic convective parameterization. *J Atmos Sci*, **59,** 959-975.

Lin, J. W. B., J. D. Neelin, and N. Zeng, 2000: Maintenance of tropical intraseasonal variability: Impact of evaporation-wind feedback and midlatitude storms. *J Atmos Sci*, **57,** 2793-2823.

Majda, A. J., and J. A. Biello, 2003: The nonlinear interaction of barotropic and equatorial baroclinic Rossby waves. *J Atmos Sci*, **60,** 1809-1821.

Matsuno, T., 1966: Quasi-geostrophicmotions in the equatorial area. *J. Meteor. Soc. Japan*, **44,** 25–43.

Mechoso, C. R., A. Kitoh, S. Moorthi, and A. Arakawa, 1987: Numerical Simulations of the Atmospheric Response to a Sea-Surface Temperature Anomaly over the Equatorial Eastern Pacific-Ocean. *Mon Weather Rev*, **115,** 2936-2956.

Neelin, J. D., and N. Zeng, 2000: A quasi-equilibrium tropical circulation model - Formulation. *J Atmos Sci*, **57,** 1741-1766.

Neelin, J. D., and H. Su, 2005: Moist teleconnection mechanisms for the tropical South American and Atlantic sector. *J Climate*, **18,** 3928-3950.

Reynolds, R. W., and T. M. Smith, 1994: Improved Global Sea-Surface Temperature Analyses Using Optimum Interpolation. *J Climate*, **7,** 929-948.

Ropelewski, C. F., and M. S. Halpert, 1987: Global and Regional Scale Precipitation Patterns Associated with the El-Nino Southern Oscillation. *Mon Weather Rev*, **115,** 1606-1626.

Salby, M. L., and R. R. Garcia, 1987: Vacillations Induced by Interference of Stationary and Traveling Planetary-Waves. *J Atmos Sci*, **44,** 2679-2711.

Saravanan, R., and P. Chang, 2000: Interaction between tropical Atlantic variability and El Nino-Southern Oscillation. *J Climate*, **13,** 2177-2194.

Sardeshmukh, P. D., and B. J. Hoskins, 1988: The Generation of Global Rotational Flow by Steady Idealized Tropical Divergence. *J Atmos Sci*, **45,** 1228-1251.

Simmons, A. J., 1982: The Forcing of Stationary Wave Motion by Tropical Diabatic Heating. *Q J Roy Meteor Soc*, **108,** 503-534.

Simmons, A. J., J. M. Wallace, and G. W. Branstator, 1983: Barotropic Wave-Propagation and Instability, and Atmospheric Teleconnection Patterns. *J Atmos Sci*, **40,** 1363-1392.

Su, H., and J. D. Neelin, 2002: Teleconnection mechanisms for tropical Pacific descent anomalies during El Nino. *J Atmos Sci*, **59,** 2694-2712.

Ting, M. F., and I. M. Held, 1990: The Stationary Wave Response to a Tropical SST Anomaly in an Idealized GCM. *J Atmos Sci*, **47,** 2546-2566.

Trenberth, K. E., G. W. Branstator, D. Karoly, A. Kumar, N. C. Lau, and C. Ropelewski, 1998: Progress during TOGA in understanding and modeling global teleconnections associated with tropical sea surface temperatures. *J Geophys Res-Oceans*, **103,** 14291-14324.

Wallace, J. M., E. M. Rasmusson, T. P. Mitchell, V. E. Kousky, E. S. Sarachik, and H. von Storch, 1998: The structure and evolution of ENSO-related climate variability in the tropical Pacific: Lessons from TOGA. *J Geophys Res-Oceans*, **103,** 14241-14259.

Wang, C. Z., S. K. Lee, and D. B. Enfield, 2007: Impact of the Atlantic warm pool on the summer climate of the Western Hemisphere. *J Climate*, **20,** 5021-5040.

——, 2008: Climate response to anomalously large and small Atlantic warm pools during the summer. *J Climate*, **21,** 2437-2450.

Wang, C. Z., S. K. Lee, and C. R. Mechoso, 2010: Interhemispheric Influence of the Atlantic Warm Pool on the Southeastern Pacific. *J Climate*, **23,** 404-418.

Webster, P. J., 1972: Response of Tropical Atmosphere to Local, Steady Forcing. *Mon Weather Rev*, **100,** 518-&.

Zeng, N., J. D. Neelin, and C. Chou, 2000: A quasi-equilibrium tropical circulation model - Implementation and simulation. *J Atmos Sci*, **57,** 1767-1796.

# List of Figures

FIG. 1. (a) The Gaussian-shaped baroclinic heating anomaly prescribed in the Atlantic Warm Pool region in QTCM, the amplitude at the center (20°N, 70°W) is equivalent to 6mm/day of precipitation (i.e., 169.2W/$m^2$). (b) The precipitation anomalies in QTCM AWP experiment, negative contour lines are dashed. The contour intervals in both are 1mm/day (the 0.5mm/day precipitation contour is shown for easier recognition of the pattern).

FIG. 2. The baroclinic streamfunction anomalies (a) and barotropic streamfunction anomalies (b) in the AWP experiment in QTCM. Negative contour lines are dashed. The contour intervals are 2 x $10^6$ $m^2$ $s^{-1}$ in (a) and 2 x $10^5$ $m^2$ $s^{-1}$ in (b).

FIG. 3. The three forcing sources in the QTCM AWP experiment: (a) shear advection; (b) surface drag; (c) vertical advection; and (d) v1 component of the surface drag (see text for explanation). Negative contour lines are dashed. The contour intervals are 2x$10^{-12}$ $s^{-2}$ within ±4x$10^{-12}$ $s^{-2}$ and 4x$10^{-12}$ $s^{-2}$ outside ±4x$10^{-12}$ $s^{-2}$ in all four panels. Shaded areas represent values that are statistically significant with a confidence level of 99% from a student's t-test.

FIG. 4. The inverse Laplacian of the three forcing sources in the QTCM AWP experiment: (a) shear advection; (b) surface drag; (c) vertical advection. Negative contour lines are dashed. The contour intervals are 1 $m^2$ $s^{-1}$ in all three. Shaded areas represent values that are statistically significant with a confidence level of 99% from a student's t-test.

FIG. 5. The barotropic streamfunction anomalies in the Eastern Pacific experiment in QTCM. Negative contour lines are dashed. The contour interval is 2 x $10^5$ $m^2$ $s^{-1}$. The shaded area is the heating prescribed in the eastern Pacific, with interval 1mm/day.

FIG. 6. (a) As in Fig. 1a, except shifting the heat source 90° in longitude to the central Pacific region. (b) Precipitation anomalies in the central Pacific experiment in the QTCM. Negative contour lines are dashed. The contour intervals are both 1mm/day.

FIG. 7. The baroclinic streamfunction anomalies (a) and barotropic streamfunction anomalies (b) in the central Pacific experiment in QTCM. Negative contour lines are dashed. The contour intervals are 2 x $10^6$ $m^2$ $s^{-1}$ in (a) and 2 x $10^5$ $m^2$ $s^{-1}$ in (b).

FIG. 8. The barotropic streamfunctions anomalies in the simple model AWP experiment (a) with shear advection; (b) with shear advection and surface drag mechanisms; (c) with shear advection and vertical advection mechanisms. Negative contour lines are dashed. The contour intervals are 2 x $10^5$ $m^2$ $s^{-1}$ in all three.

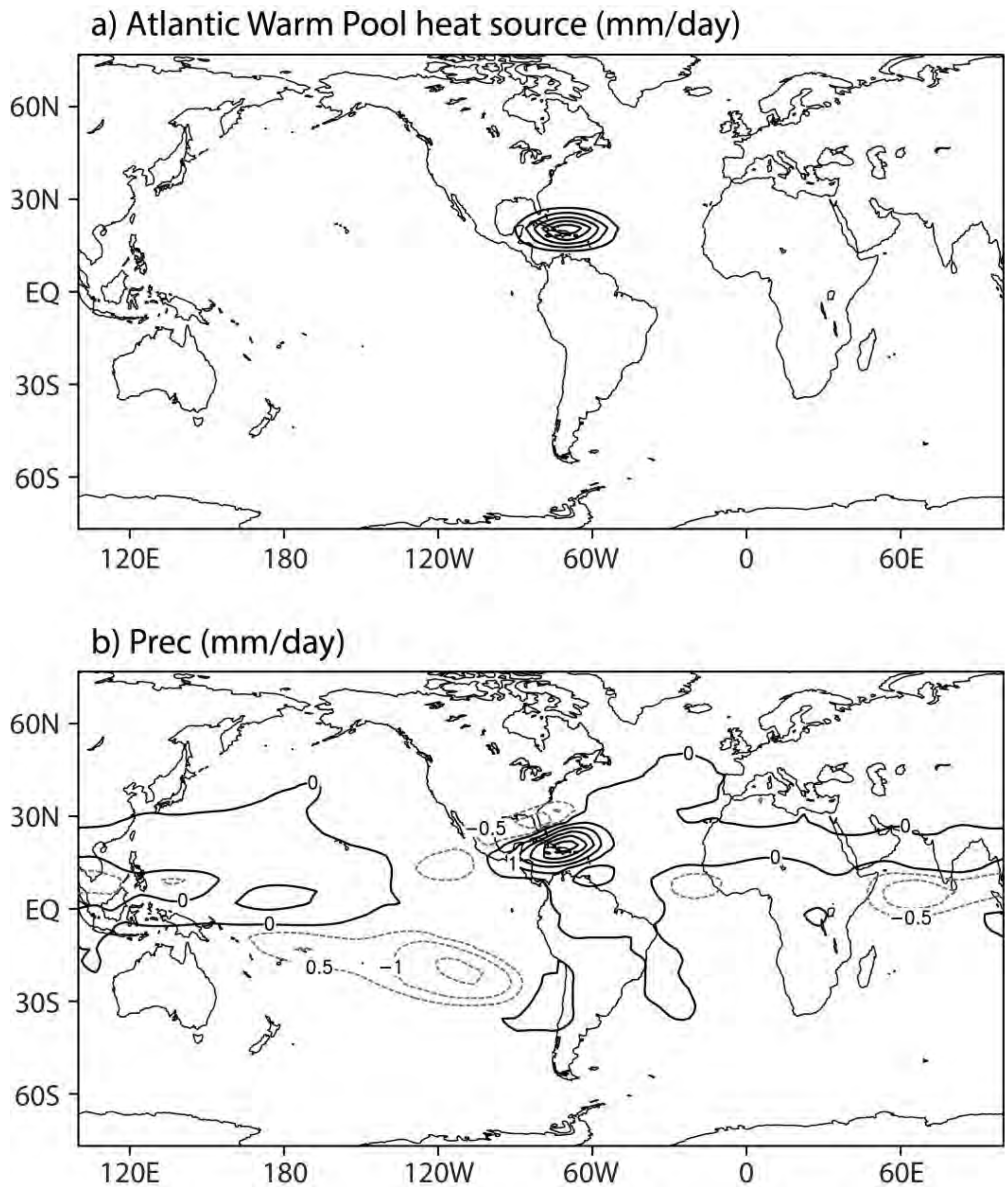


FIG. 1. (a) The Gaussian-shaped baroclinic heating anomaly prescribed in the Atlantic Warm Pool region in QTCM, the amplitude at the center (20°N, 70°W) is equivalent to 6mm/day of precipitation (i.e., 169.2W/$m^2$). (b) The precipitation anomalies in QTCM AWP experiment, negative contour lines are dashed. The contour intervals in both are 1mm/day (the 0.5mm/day precipitation contour is shown for easier recognition of the pattern).

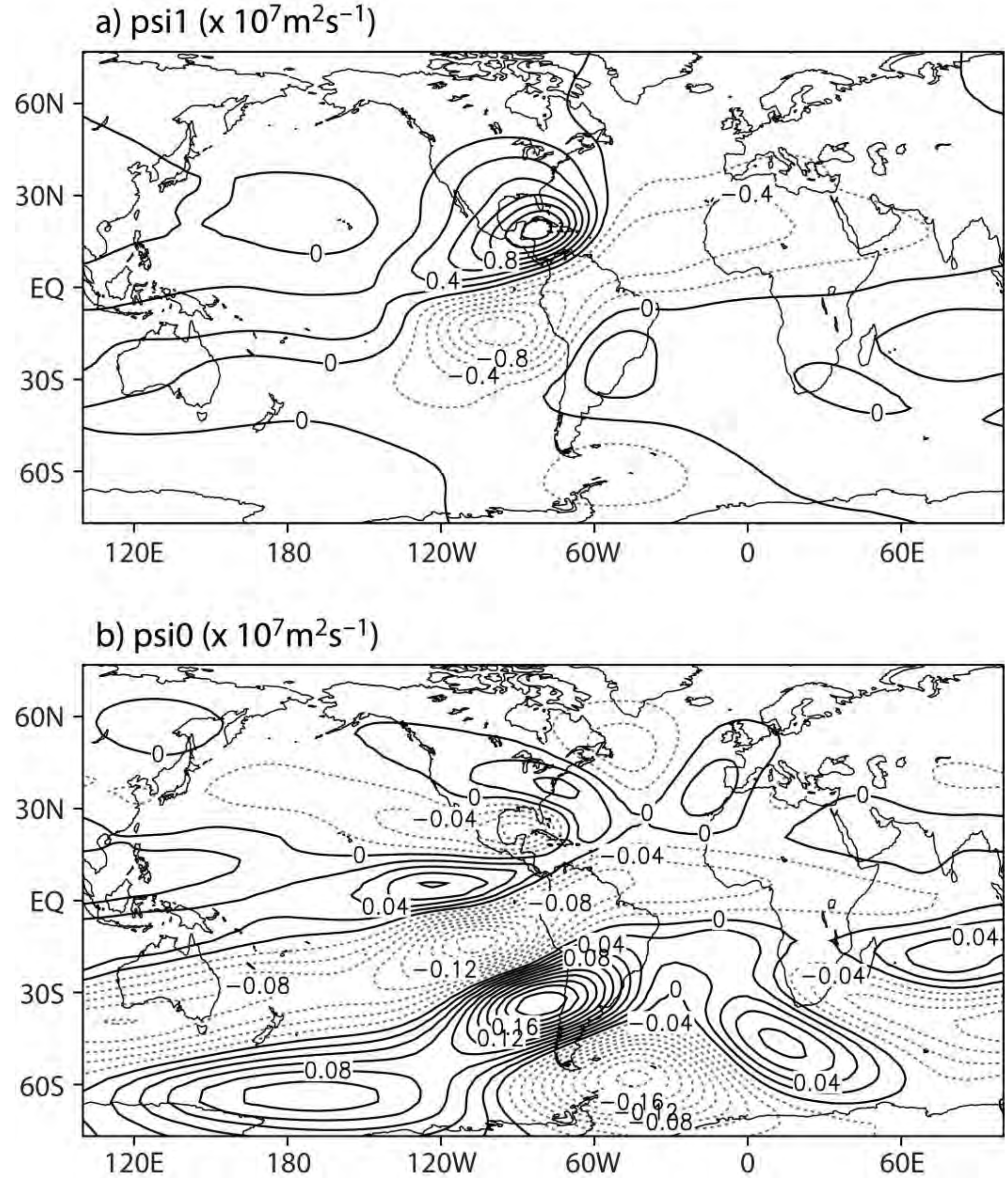


FIG. 2. The baroclinic streamfunction anomalies (a) and barotropic streamfunction anomalies (b) in the AWP experiment in QTCM. Negative contour lines are dashed. The contour intervals are 2 x $10^6$ $m^2$ $s^{-1}$ in (a) and 2 x $10^5$ $m^2$ $s^{-1}$ in (b).

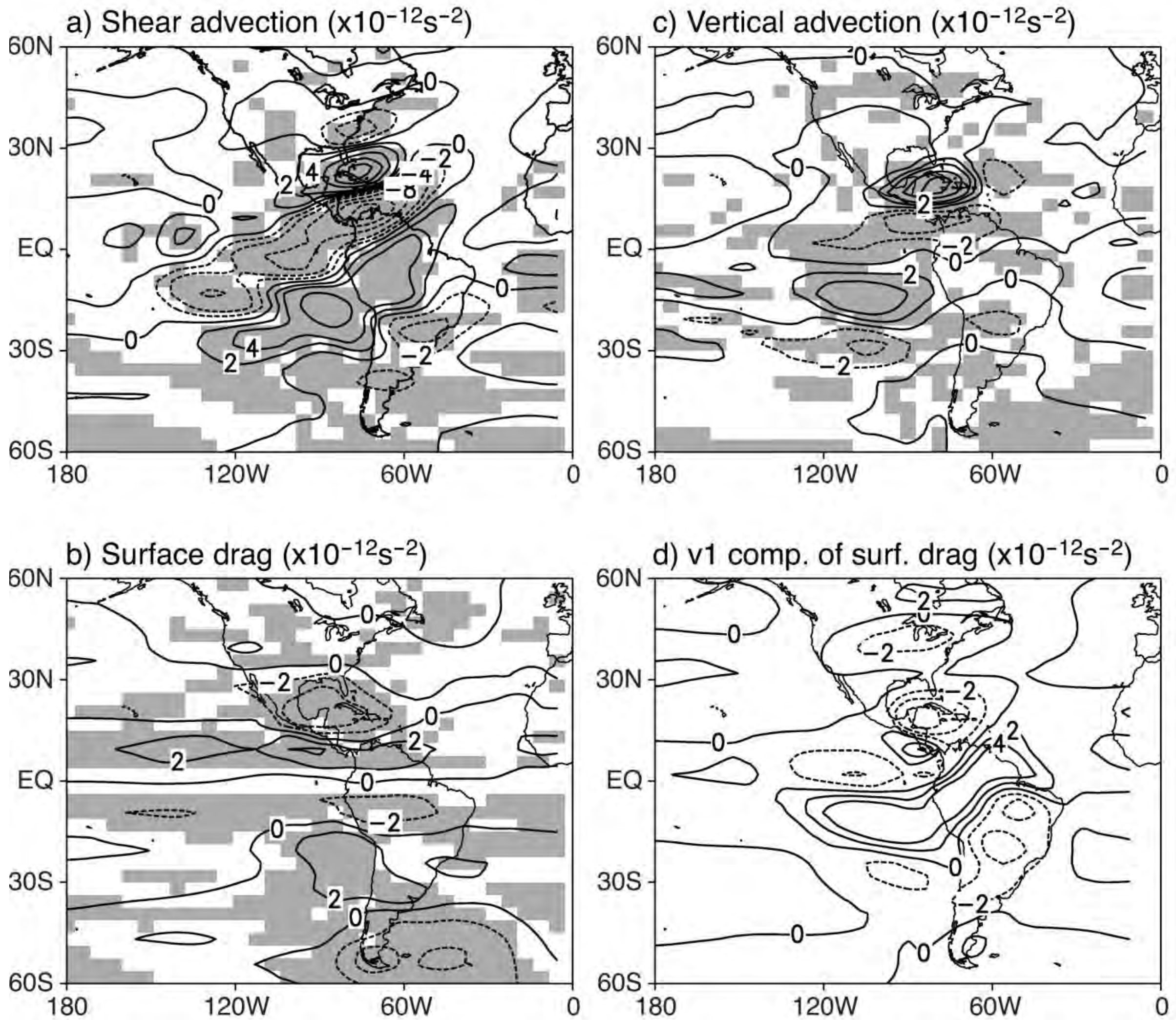


FIG. 3. The three forcing sources in the QTCM AWP experiment: (a) shear advection; (b) surface drag; (c) vertical advection; and (d) v1 component of the surface drag (see text for explanation). Negative contour lines are dashed. The contour intervals are $2\text{x}10^{-12}$ $s^{-2}$ within $\pm4\text{x}10^{-12}$ $s^{-2}$ and $4\text{x}10^{-12}$ $s^{-2}$ outside $\pm4\text{x}10^{-12}$ $s^{-2}$ in all four panels. Shaded areas represent values that are statistically significant with a confidence level of 99% from a student's t-test.

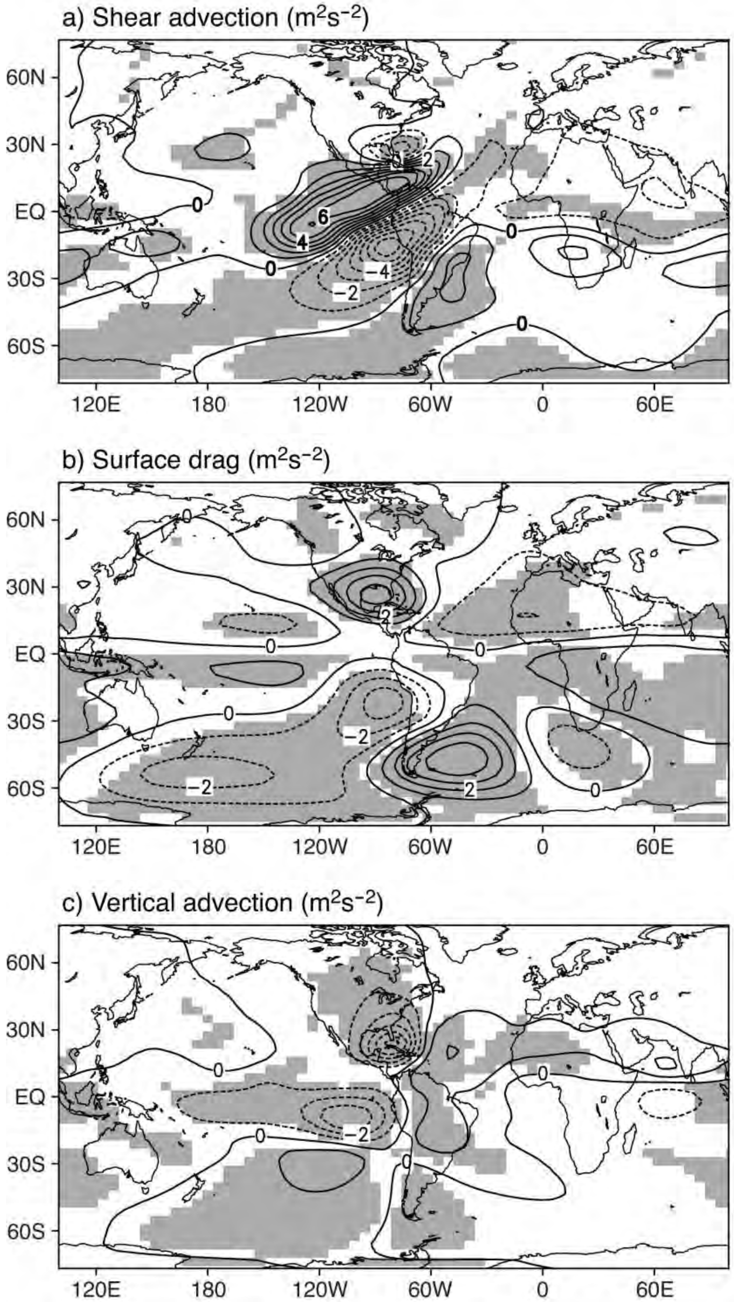


FIG. 4. The inverse Laplacian of the three forcing sources in the QTCM AWP experiment: (a) shear advection; (b) surface drag; (c) vertical advection. Negative contour lines are dashed. The contour intervals are 1 $m^2$ $s^{-1}$ in all three. Shaded areas represent values that are statistically significant with a confidence level of 99% from a student's t-test.

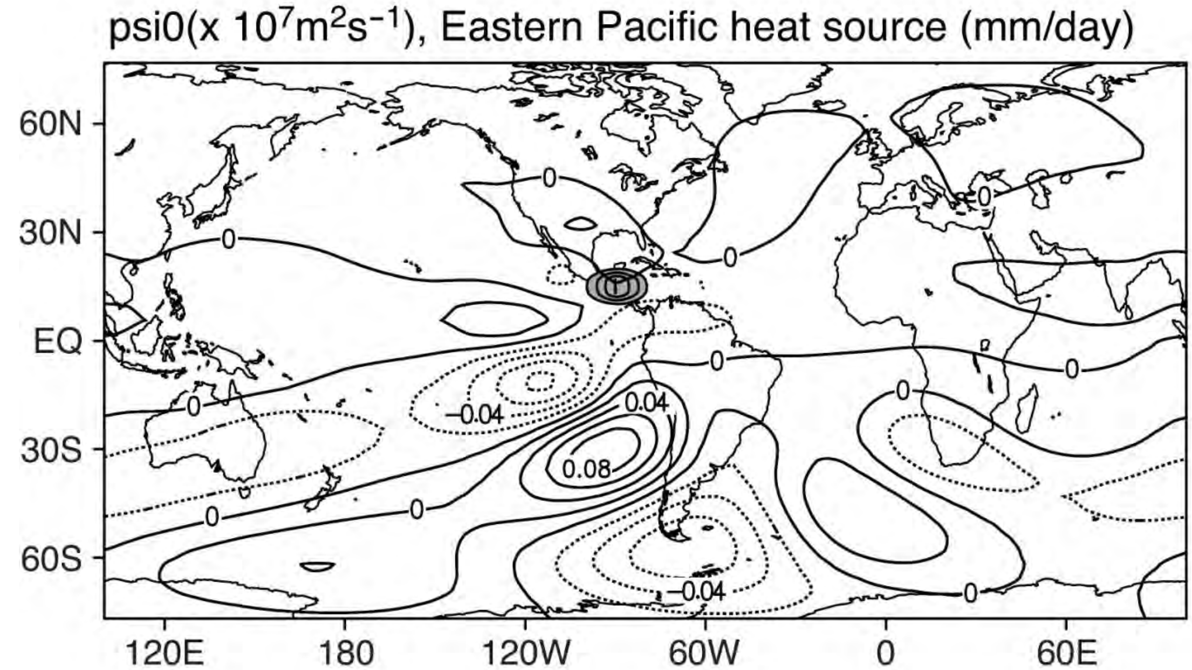


FIG. 5. The barotropic streamfunction anomalies in the Eastern Pacific experiment in QTCM. Negative contour lines are dashed. The contour interval is 2 x $10^5$ $m^2$ $s^{-1}$. The shaded area indicates the heating prescribed in the eastern Pacific, with interval 1mm/day.

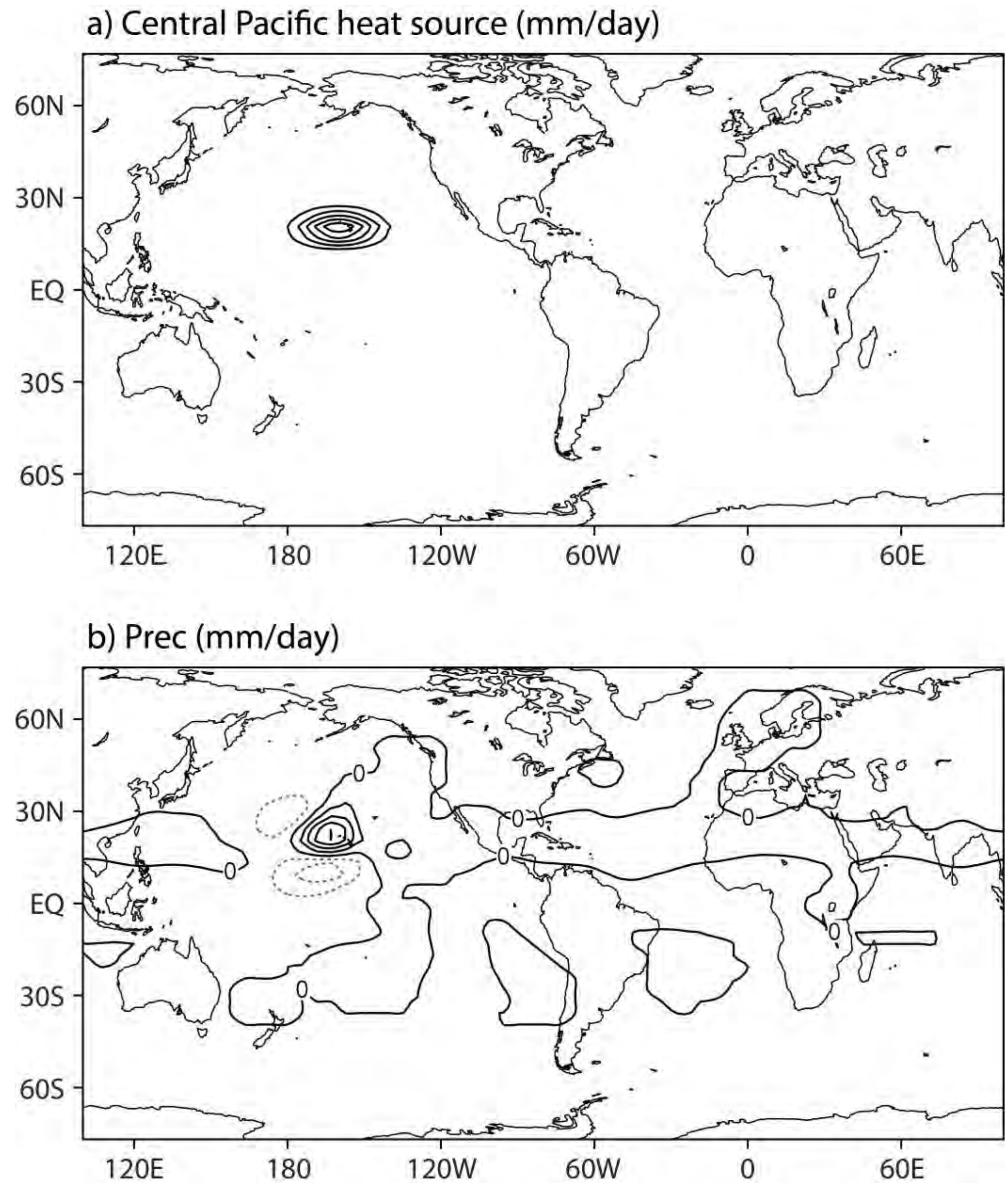


FIG. 6. (a) As in Fig. 1a, except shifting the heat source 90° in longitude to the central Pacific region. (b) Precipitation anomalies in the central Pacific experiment in the QTCM. Negative contour lines are dashed. The contour intervals are both 1mm/day.

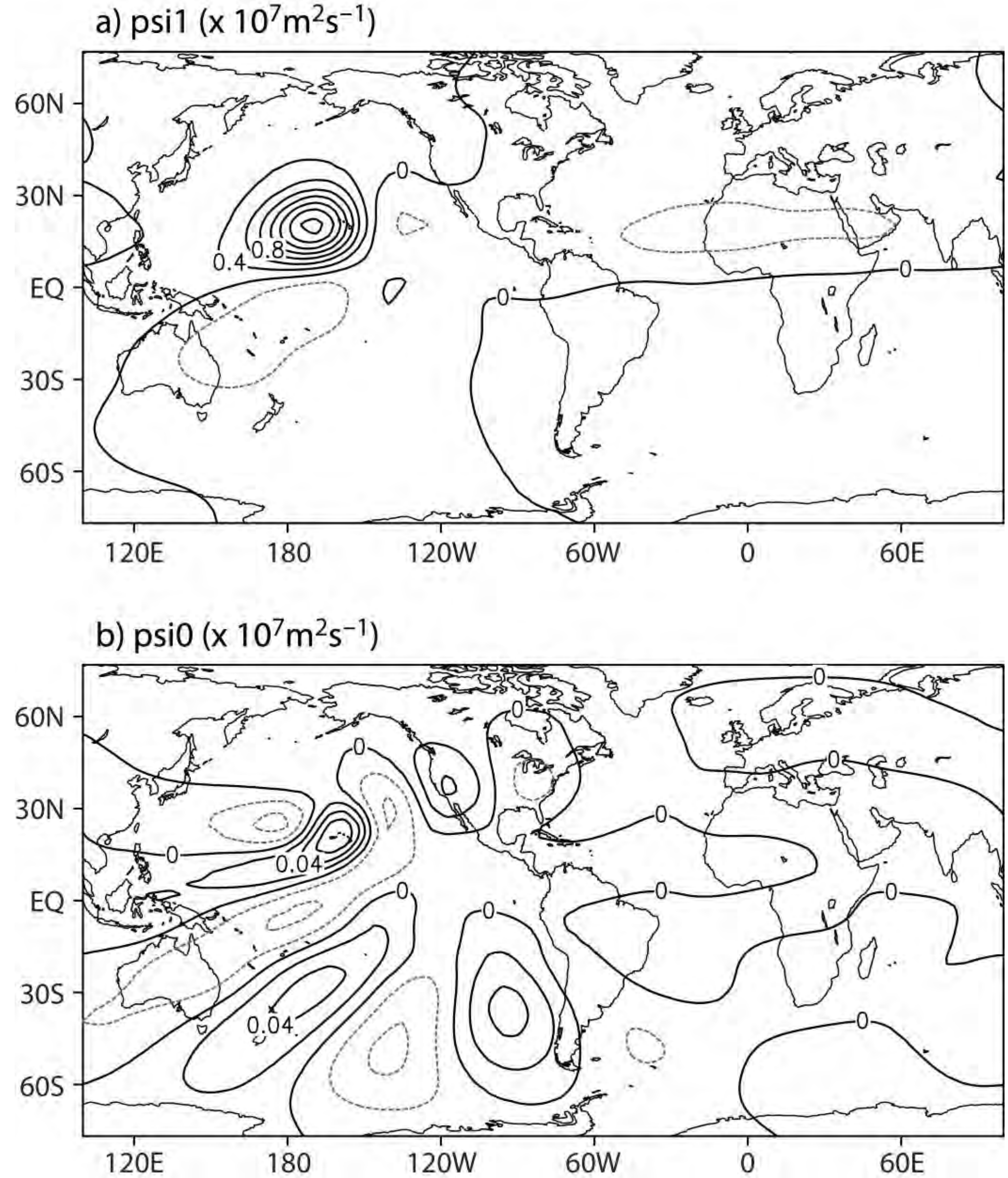


FIG. 7. The baroclinic streamfunction anomalies (a) and barotropic streamfunction anomalies (b) in the central Pacific experiment in QTCM. Negative contour lines are dashed. The contour intervals are 2 x $10^{6}$ $m^{2}$ $s^{-1}$ in (a) and 2 x $10^{5}$ $m^{2}$ $s^{-1}$ in (b).

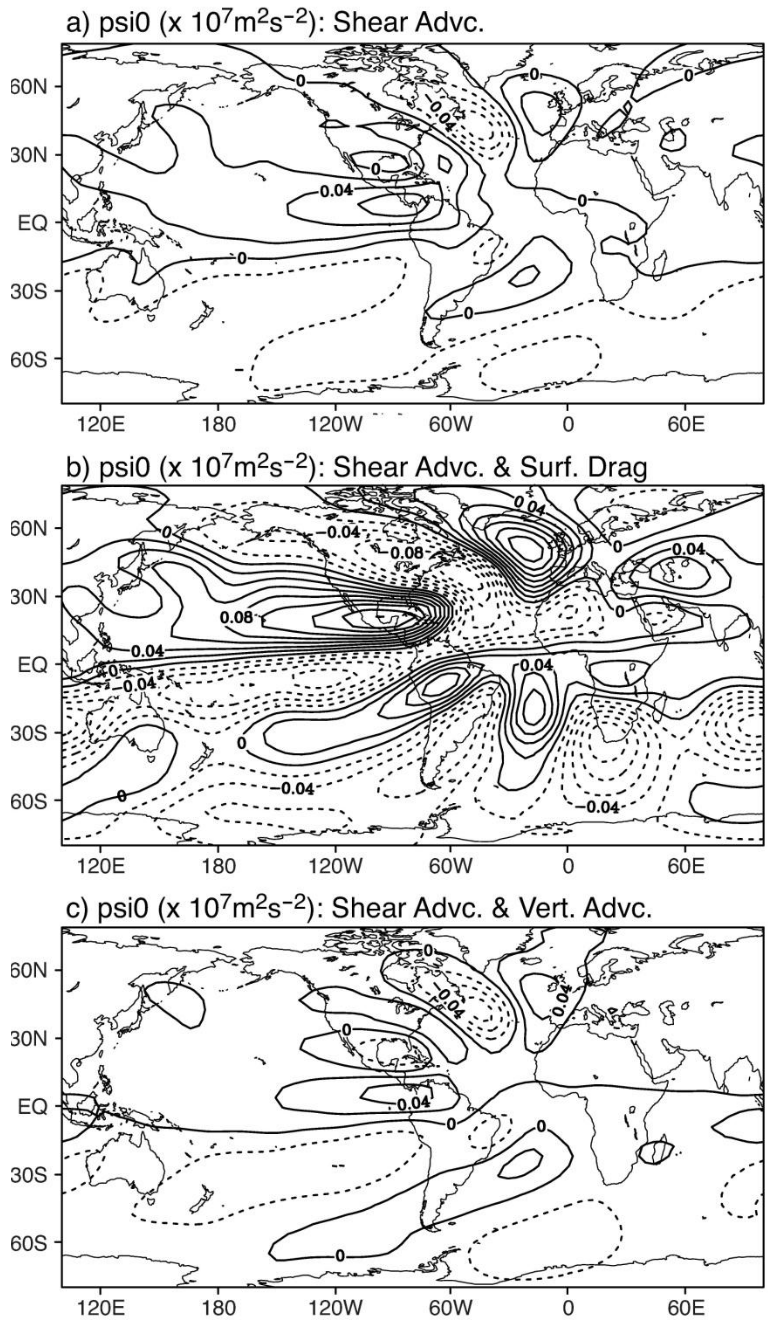


FIG. 8. The barotropic streamfunctions anomalies in the simple model AWP experiment (a) with shear advection; (b) with shear advection and surface drag mechanisms; (c) with shear advection and vertical advection mechanisms. Negative contour lines are dashed. The contour intervals are $2 \times 10^5$ $m^2$ $s^{-1}$ in all three.